SQUID-based ULF MRI and Superparamagnetic Relaxometry for Early Cancer Diagnostics

Andrei N. Matlashov, Per E. Magnelind, Young Jin Kim, Henrik Sandin, Aaron Anderson, Harshini Mukundan, and Michelle A. Espy

Los Alamos National Laboratory, Los Alamos, NM 87545, USA
e-mail: matlach@lanl.gov

***Abstract*—Ultra-sensitive detection and imaging of tagged tissue cells using superparamagnetic nanoparticles is a developing technique for early cancer diagnostics. SQUIDs are very suitable for such sensitive measurements. Relaxometry is used for detection of tagged cells with high specificity, as only bound nanoparticles are detected via Néel relaxation. By combining relaxometry with magnetic resonance imaging the tagged area can be imaged to provide information for the inverse problem solution. Such combination could provide both accurate localization and cell count of the tagged tissue, which would enable detection and localization of cancerous tissue at a very early disease stage.**

Manuscript received July 18, 2013. Accepted July 20, 2013. Reference No. ST342; Category 4.
Preprint of a paper presented at ISEC 2013.

***Keywords* – SQUID, MRI, relaxometry, early cancer detection, magnetic nano-marker.**

I. INTRODUCTION

Colloidal solutions of superparamagnetic particles of typical 10-30 nm size, called ferrofluids, can be used in medicine as contrast agents for magnetic resonance imaging (MRI) and also as nano-markers for tagging specific cells such as cancerous cells. The first use of SQUIDs for detection of magnetic nano-markers in biological samples was proposed by Kötitz and colleagues in 1994 [1]. This method was named SQUID magnetorelaxometry or MRX [2]. Tagging specific cells with superparamagnetic nano-markers with subsequent SQUID-based relaxometry allows detection and localization of very small quantities of cells. Early detection of cancer cells is vital in minimizing the risk of entering a metastatic phase [3, 4]. The detection limit of this technique is estimated to be as low as 10,000 cells, which is 2 orders of magnitude lower than for state of the art spiral X-ray CT [5]. Low-level cell detection can also be used for nonsurgical determination of organ transplant conditions using T-cell labeling [6], or for early diagnostic of Alzheimer's and other neurological diseases [7].

Recently, advancements in biomarkers and nano-technology, e.g. the production of very uniform and stable single core magnetic nanoparticles labeled with specific bioagents, have made this promising method practical as a cancer diagnostic. Precise size and magnetic permeability allow researchers to pre-magnetize particles and measure the

remnant magnetic moment during Néel relaxation of the particles [8]. A measurable magnetic field featuring a few seconds relaxation time is generated only by immobilized nanoparticles of a specific size.

The magnetic moment of the tagged tissue cannot be calculated from a single decay signal without knowing its exact spatial position. Thus, a multichannel system should be used that provides decay signals in several spatial positions simultaneously, enabling the magnetic moment and its localization to be estimated using a magnetic dipole source model fitting routine. Such a routine provides an estimated position and magnitude of the magnetized tagged volume using an ill-posed inverse problem solution. To obtain more accurate localization and spatial distribution for the tagged region ultra-low field magnetic resonance imaging (ULF MRI) can be used, which also relies on sensitive SQUID detection. The spatial information obtained from ULF MRI can then be used for the magnetic moment calculation to give the number of tagged cells. SQUID relaxometry has never before been combined with MRI using a single device. The first published results of experimental comparison of these two methods used two separate instruments: a conventional 4.7 T MRI system and a SQUID-based system [9]. In this paper we demonstrate the possibility of combined magnetic relaxometry and ULF MRI of phantoms recorded using one 7-channel SQUID-gradiometer system.

II. EXPERIMENTAL METHODS

The design of the system has been described in detail elsewhere [10]. In brief, the system consists of seven axial second-order wire-wound gradiometers 37 mm diameter and 60 mm baseline. The gradiometers are positioned in parallel one in the middle and six others surrounding it in a hexagonal pattern with 45 mm separation between the axes. The magnetic field noise spectral density referred to one pick-up turn is below 2.5 fT/√Hz for all channels. All experiments described here were performed inside a two-layer magnetically shielded room (MSR).

ULF MRI was performed using a field-cycling and spin-echo protocol similar to the description in [11]. A 2D Fourier imaging protocol was used to demonstrate the properties of the magnetic nanoparticles as a contrast agent, when immersed in agarose as a surrogate for tissue. We also wanted to know how much the MRI relaxation of pure agarose differs from water. Experiments were performed with a frequency encoding gradient 150 μT/m and phase encoding gradient in 55 steps between maximal positive and negative values 154 μT/m. The resulting pixel size was 3×3 mm^2 with 160 mm diameter field of view. The encoding and acquisition times were 25 ms and 50 ms, respectively. The measurement field of about 96 μT was generated by a 122 cm diameter Helmholtz system.

The 1400-turn pre-polarization coil was cooled by liquid nitrogen. Its dimensions were OD 300 mm, ID 100 mm and height 100 mm. It was placed co-axial with the central gradiometer about 100 mm below its bottom pick-up coil. This coil generated a 3.42 mT/A pre-polarization field in a phantom position 30 mm above the upper coil surface. For MRI we pre-polarized using a 15 A current supplied by two Techron 7780 amplifiers with adiabatic ramp-down. The same coil was also used for magnetic relaxometry measurements using a 5.5 mT magnetizing field. Cryogenic switches were used to disconnect SQUIDs from gradiometers during the time when a large field was applied and cycled.

The phantoms were prepared using small (~1 ml), medium (~5 ml), and large (~15 ml) vials placed in a large dish of water, 140 mm ID and 45 mm deep. Agarose with uniformly embedded iron oxide nanoparticles, 30 nm size magnetite SMG30 from Ocean NanoTech at ~ 7×10^{11} per 1 ml, was used to fill the medium and small vials. The large vial did not contain a significant quantity of nanoparticles. We assumed that agarose kept some fraction of nanoparticles immobilized allowing only Néel relaxation in the case of magnetic relaxometry, simulating the conditions for particles bound to cells. In the case of ULF MRI, the same nanoparticles should work as a contrast agent. We also assumed that our smallest phantom would behave as a magnetic dipole in the case of magnetic relaxometry.

A 3D Fourier imaging protocol was used to localize the small vial placed inside a dish of water. Additional phase encoding gradient in 9 steps between maximal positive and negative values 90 μT/m was used for the third dimension. A four-echo imaging sequence was implemented that can be used to highlight the contrast caused by the nanoparticles. Magnetic relaxation was done immediately after imaging with exactly the same phantom position.

Magnetic relaxation was performed using a 5.5 mT magnetizing field applied for 1 s followed by a 3 ms switch-off. The magnetic field relaxation signal recording started about 12 ms after the magnetizing field was zeroed. The relaxation signal from nanoparticles was masked by large transient signal coming from the MSR walls. It was possible to suppress the transient by about 5 times using a 1 m diameter compensation coil placed close to the MSR ceiling. A baseline was recorded without a phantom and subtracted from the signal recorded with a phantom in place. This difference reveals the relaxation signal primarily from the nanoparticles. Raw relaxation signals were fitted using a logarithmic function, $f_{fit}=a_1\ln(1+a_2/t)+a_3$, where a_i are fitting parameters and t is the time, in the area of slow signal decay and a 5^{th}-order polynomial fit of the early relaxation curve for extrapolation to time zero when the command was sent to switch off the magnetizing field. A dipole approximation was used for single vial localization and the magnetic moment was estimated using an inverse problem solution.

III. RESULTS

The main goal of this work was to demonstrate ULF MRI and magnetic relaxometry using the same SQUID-based instrument. ULF MR imaging is a technically more complex method than magnetic relaxometry. It needs a much stronger pre-polarization field and many signal controls. However the conventional signal processing is straightforward and gives final volume distribution of nanoparticles. In our preliminary ULF MRI measurements we tested the efficacy of magnetic nanoparticles as a contrast agent using a phantom with the large vial filled with pure agarose and the medium vial filled with agarose containing uniformly distributed nanoparticles. Fig. 1 shows a 2D MR density image of this phantom. Although it is not a T_2-weighted MR image one can clearly see weak contrast in the case of the large vial with agarose and more visible contrast of the vial with nanoparticles. The differences in contrast arise from T_2 effects. We note that the two black spots in the center and top of the image are air bubbles.
It improves uniformity and contrast of the images.

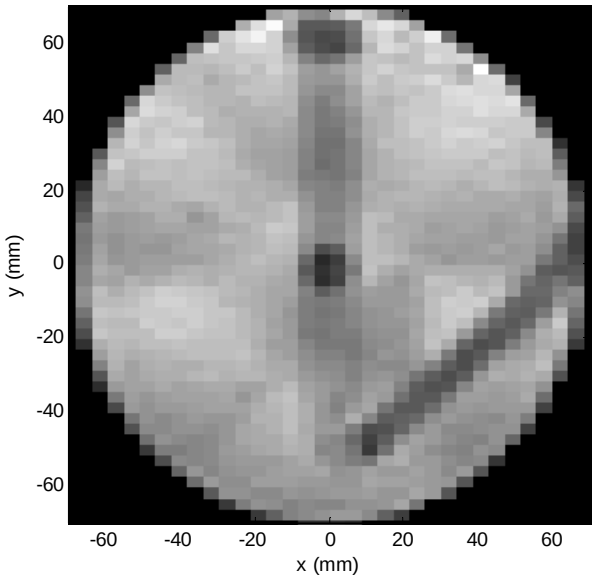

Fig. 1. Ultra-low field 2D MR image of a phantom with two vials: ID 15 mm, L 120 mm vial without NP (vertical along *y*-coordinate) and ID 10 mm, L 75 mm (tilted on the right bottom quadrant) filled with 30 nm SMG30 magnetic nanoparticles with a concentration of ~ 7×10^{11} per 1 ml. Such normalization improves uniformity and contrast of the images.

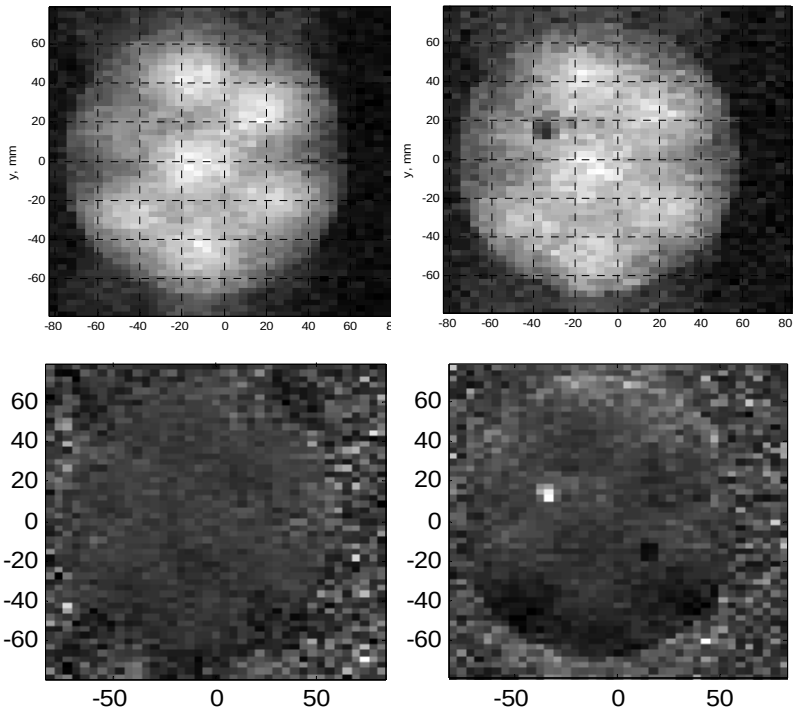

Fig. 2. Top row: Left shows an image of the phantom at a depth of 20 mm. Right shows an image at a depth of 25 mm, containing the vial with nanoparticles. The image on the right clearly shows the effects of the nanoparticles on relaxation. Lower row: The left and right show corresponding images to those in the top row, normalized to a sensitivity map obtained by imaging the phantom rotated by 180 degrees.

A 3D localization experiment was done using a phantom with the small vial immersed in the dish of water. The vial contained about 10^{12} nanoparticles that corresponds to 1 mm size labeled tumor. The vial upper surface was placed 20 mm below water surface and about 25 mm below the cryostat surface, which corresponds to zero position in vertical direction. In the horizontal plane it was between channels 1 (blue), 4 (light blue) and 5 (magenta). The upper row in Fig. 2 shows two slices corresponding to depths of 20 mm (not containing the vial) at left and 25 mm (containing the vial) at right. The voxel size on images is $3\times3\times5$ mm^2. The black spot on image at 25 mm (upper right) is the vial. The bottom row shows the same two images with each voxel divided by a corresponding voxel from a sensitivity map obtained by imaging the same phantom rotated by 180 degrees.

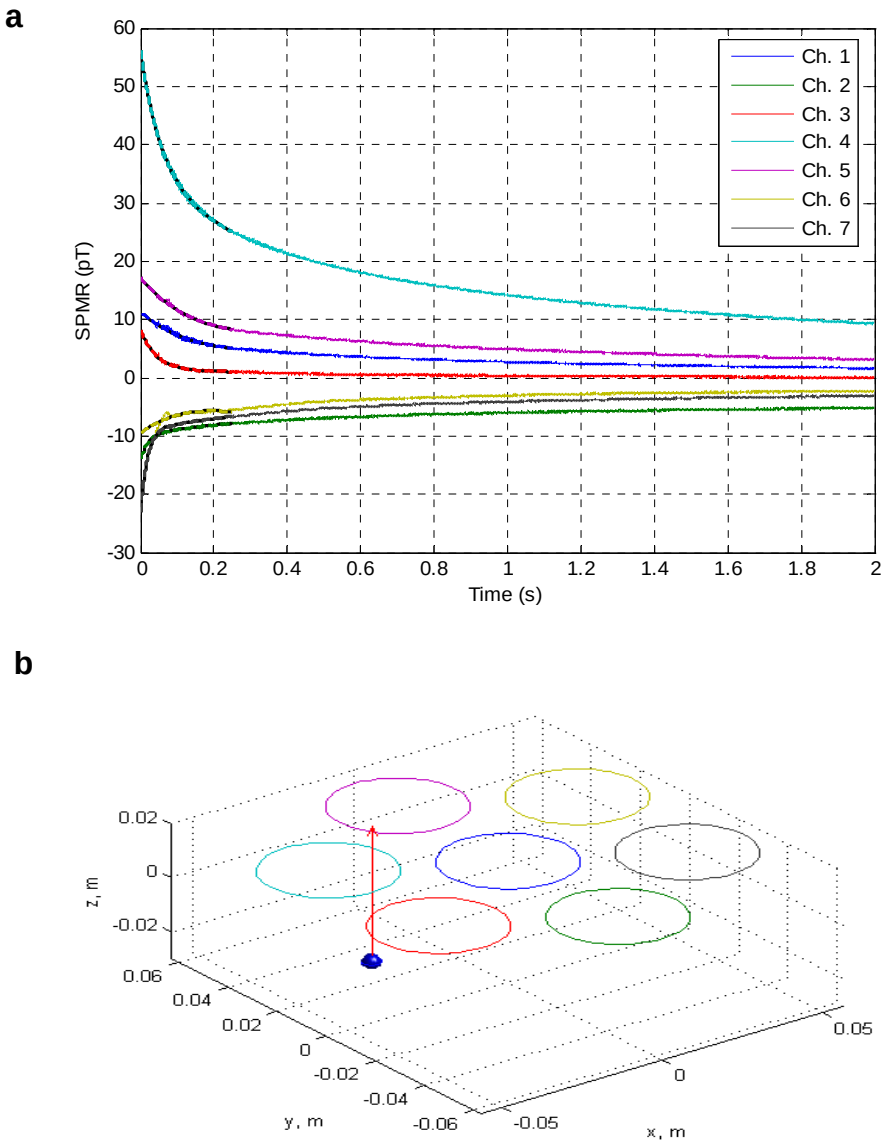

Fig. 3. a) Seven magnetic relaxation signals recorded from 1 ml vial, ID 10 mm, L 15 mm, and containing ~10^{12} nanoparticles that corresponds to 1 mm size labeled tumor, placed 20 mm below the water surface. b) The dipole localization using an inverse problem solution. The calculated dipole coordinates are $x = -24.0$ mm, $y = 20$ mm, $z = -24.8$ mm.

The magnetic relaxometry experiment was done using the same phantom immediately after imaging. Seven relaxation signals are shown in Fig. 3(a). An inverse problem solution using a single dipole approximation gives the vial center position: x = −24.0 mm, y = 20 mm, z = −24.8 mm with a magnetic moment estimated equal to 5×10^{-10} J/T. The position localized by the relaxation signals agrees well with the physical location of the vial, as well as its location in the MRI. Fig. 3(b) shows the calculated dipole position with respect to gradiometer pick-up coils.

Using seven spatial points we were able to localize a single dipole source. However, for an extended source or for multiple sources the localization needs significantly more measurement positions (or channels) [3] or additional constraints on the inverse problem solution. Input from ULF MR images can provide this spatial information as well as anatomical context and localization constraints. This will reduce the required number of channels and provide realistic spatial bounds for the inverse problem solution. Without ULF MRI data, magnetic relaxation may cause unacceptable error in magnetic moment estimation, i.e. in counting cancerous cells.

IV. CONCLUSION

Here we present the possibility of combining magnetic relaxometry and ULF MRI in a single instrument. An image showing the influence of the nanoparticles as a contrast agent was obtained, and a plausible fit (assuming a single dipole model) for the location and strength of a magnetic dipole was obtained by magnetic relaxometry. This work indicates the feasibility of a single system for such measurements. Future work will focus on using the MRI to constrain multiple dipole fitting. The combination of MRI with magnetic relaxometry will clearly improve our ability to accurately estimate and localize magnetic dipoles, with direct impact on the efficacy of the technique of superparamagnetic relaxometry as a sensitive early cancer diagnostic.

ACKNOWLEDGMENT

The authors would like to thank Dr. Edward Flynn and Dr. John George for their significant support. The authors also thank Petr Volegov for his data analysis tools that were invaluable in the creation of the algorithms for this work. We gratefully acknowledge the support from LANL's LDRD office through the grants 20100097DR and 20130624ER.

REFERENCES

[1] R. Kötitz, L. Trahms, H. Koch, and W. Weitschies, "Ferrofluid relaxation for biomagnetic imaging," in Biomagnetism: Fundamental Research and Clinical Applications, C. Baumgartner, L. Deecke, G. Stroink, S. J. Williamson, Eds. Amsterdam: Elsevier, 1995, pp. 785-788.

[2] R. Kötitz, et al., "Detection of biodegradation of ferrofluid by relaxation methods," in Biomag 96, C. J. Aine, Y. Okada, G. Stroink, S. J. Swithenby, C. C. Wood, Eds. Berlin: Springer, 2000, pp. 655-658.

[3] H. J. Hathaway, et al., "Detection of breast cancer cells using targeted magnetic nanoparticles and ultrasensitive magnetic field sensors," Breast Cancer Res., vol. 13, R108(13 pages), 2011.

[4] E. R. Flynn, et al. "Application of Magnetic Relaxometry in Ovarian Cancer Nanomedicine," in press

[5] E. R. Flynn and H. C. Bryant, "A biomagnetic system for *in vivo* cancer imaging," *Phys. Med. Biol.*, vol. 50, pp. 1273-1293, 2005.

[6] E. R. Flynn, et al., "Use of a SQUID array to detect T-cells with magnetic nanoparticles in determining transplant rejection," J. Magn. Magn. Mater., vol. 311, pp. 429–435, 2007.

[7] E. R. Flynn, "Biomagnetic detection and treatment of Alzheimer's disease," US Patent 8060179 B1, 2011.

[8] L. Néel, "Some theoretical aspects of rock-magnetism," Adv. Phys., vol. 4, pp. 191–243, 1955.

[9] N. L. Adolphi, et al., "Detection and Imaging of Her2-Targeted Magnetic Nanoparticles: Direct Comparison of SQUID-detected Magnetic Relaxometry and Magnetic Resonance," Contrast Media Mol. Imaging, vol. 7, pp. 308–319, 2012.

[10] V. S. Zotev et al. "Multi-channel SQUID system for MEG and Ultra-Low Field MRI," IEEE Trans. Appl. Supercond., vol. 17, no. 2, pp. 839-842, 2007.

[11] M. A. Espy et al. "Toward high-resolution images with SQUID-based ultra-low field magnetic resonance imaging," IEEE Trans. Appl. Supercond., vol. 23, no. 3, p. 1603107, 2013.